Molecular Crystals and Liquid Crystals
Publication details, including instructions for authors and subscription information:
http://www.tandfonline.com/loi/gmcl20

3D Modeling of Single-Domain and Multi-Domain Vertical Alignment LCDs for Direct-View and Microdisplay Geometries

C. Y. Yin [a], I-Lin Ho [a], Y. C. Chang [a] & Hiap L. Ong [b]
[a] Research Center for Applied Sciences, Academia Sinica, 128 Academia Road, Section 2, Nankang, Taipei, 115, Taiwan (ROC)
[b] Kyoritsu Optronics Co., Ltd., 7 Fl, No. 38-6. Tian Mu East Road, Taipei, 111, Taiwan (ROC)
Version of record first published: 13 Jun 2012.

To cite this article: C. Y. Yin , I-Lin Ho , Y. C. Chang & Hiap L. Ong (2012): 3D Modeling of Single-Domain and Multi-Domain Vertical Alignment LCDs for Direct-View and Microdisplay Geometries, Molecular Crystals and Liquid Crystals, 561:1, 203-224

To link to this article: http://dx.doi.org/10.1080/15421406.2012.687239

Mol. Cryst. Liq. Cryst., Vol. 561: pp. 203–224, 2012

ISSN: 1542-1406 print/1563-5287 online
DOI: 10.1080/15421406.2012.687239

Taylor & Francis
Taylor & Francis Group

3D Modeling of Single-Domain and Multi-Domain Vertical Alignment LCDs for Direct-View and Microdisplay Geometries

C. Y. YIN,[1] I-LIN HO,[1] Y. C. CHANG,[1,*]
AND HIAP L. ONG[2]

[1]Research Center for Applied Sciences, Academia Sinica, 128 Academia Road, Section 2, Nankang, Taipei 115, Taiwan (ROC)
[2]Kyoritsu Optronics Co., Ltd., 7 Fl, No. 38–6. Tian Mu East Road, Taipei 111, Taiwan (ROC)

We successfully developed a 3D liquid crystal display (LCD) modeling program and applied the program to modeling the single-domain vertical alignment (VA) and intrinsic fringe field controlled multi-domain vertical alignment (IFF MVA) LCDs. Our study showed that proper and stable IFF MVA operation was obtained in the microdisplay geometry but not in the direct-view geometry, whereas regular VA operation was obtained in the direct-view geometry but not in the microdisplay geometry.

Keywords cross-talk; disclination; fringe field; 3D modeling; microdisplay; multi-domain vertical alignment

I. Introduction

Liquid crystal displays (LCDs) are now mature displays with high-quality optical performance, such as high optical transmission, high contrast ratio (CR), large symmetrical viewing angle, high resolution, and low cross-talk. However, severe product competition and emergence applications require continuous and significance improvements on the LCD performance and technology development. Therefore, there is a continued need for the fast and accurate modeling program for LCD characterization and improvement. There are a numbers of 1D and 2D, as well as 3D LCD modeling programs, such as the Tech Wiz [1], Expert LCD [2], DIMOS [3] and LCD MASTER [4]. At present, these LCD modeling programs are for the LC electro-optical effects with the 3D LC spatial structures, but do not consider the 3D LC visual performances.

Recently, we developed a 3D LCD visual system using MVA LCDs which combined the LC electro-optical effects with the 3D LCD visual system for 3D LCD applications. We then developed a 3D LCD modeling program to calculate the 3D LCD orientation and their corresponding electro-optical properties for high-performance MVA and 3D LCD applications. We applied our 3D LCD modeling program to model the intrinsic fringe field controlled multi-domain vertical alignment (IFF MVA) and vertical alignment (VA)

*Address correspondence to Y. C. Chang, Research Center for Applied Sciences, Academia Sinica, 128 Academia Road, Section 2, Nankang, Taipei 115, Taiwan (ROC). Tel: 886-2-2782-6627; Fax: 8 886-2-27826672. E-mail: yiachang@gate.sinica.edu.tw

LCDs, for both large and small pixel geometries [5]. We focused in particular on the microdisplay display geometry and made detailed comparisons on performance versus the display driving scheme and the large pixel geometry. It is important to study the performance versus display driving scheme and pixel size because of the existence of fringe field and the induced disclination effects. The comparison between the small and large pixel geometries will help us understand the disclination and the cross-talk induced by the fringe field effects and their impact on the optical performance.

In conventional direct-view LCDs, the display dot sizes are typically 150×450 μm for the LC TV, 60×180 μm for the typical small-medium size LCDs, 35×105 μm for the high-end smart phone and 26×78 μm for the typical retina displays. Microdisplays are characterized by their very small pixel sizes, typically smaller than 15×15 μm for current microdisplays, and microdisplays with a dot size of 2.8×8.4 μm are now available for the high-end electronic view-finder applications [6, 7]. Because of the very small dot size, to view the contents of these LCDs all microdisplays require an optical enlargement system such as magnifying lens or projection systems. The smaller form factor offers distinct advantages for higher resolution in small LCD, lower cost, less weight, lower power consumption and more compactness. The applications include electronics view-finder (EVF), digital camera, camcorder, integrated Eyeglass, personal WEB browser, hand-held GPS, personal DVD viewer, projector, and head-mounted displays. These are important for consumer, industry and military applications. Recently, there is a growing interest for the applications of pico-projector using microdisplays.

II. 3D LCD Modeling Program Setup

II.1 3D LCD Modeling Program

In our 3D LCD modeling program, the Q-tensor model of Frank-Oseen elastic energy density has been employed to calculate the interaction between the electric field and LC molecules [8, 9]. Compared with the Landau-de Gennes's Q-tensor model, the vector approach is relatively faster because its formula is simpler. The shortcoming of the vector model is that sometimes it yields inaccurate results due to discontent of "inversion symmetry" or the so called "the n and $-$n equivalence" [10]. Landau-de Gennes's Q tensor approach fulfills the "inversion symmetry" representing the characteristic of LC molecules that allows us to get accurate results of 3D distribution of LC orientations. Furthermore, in order to get more accurate results, thermal fluctuations effects dynamically modeled by a Gaussian-type moving average process for LC are included in our 3D modeling program. [11] We have also included the rigorous coupled wave analysis (RCWA) in the program for the calculation of light diffraction effects [12].

Each dot is divided into grid points and the size of each grid point is 0.1×0.1 μm, with a 6×2 dot layout and periodic boundary conditions. After analyzing LC dynamics, the extended 2×2 Jones matrix method (JMM) has been employed to calculate the optical field modulated by LC. [13, 14] This JMM method can be used for different kinds of LCD systems which include TN, STN, VA, MVA and amplified intrinsic fringe field (AIFF) types with birefringent materials in an arbitrary arrangement of LC structures. [15–18]

II.2 Pixel and LC Parameters

In this paper, we report on two 3D LCD simulations for the VA and IFF MVA LCDs for microdisplay geometry of a dot size of 3.75×11.25 μm and for direct-view geometry of a

dot size of 63.2×189.6 μm. The aperture ratio is 60%, thus the opening areas are 2.85×8.50 μm and 49.20×147.60 μm respectively for the two LCD geometries.

Merck VA LC MJ021866 is used in the modeling with the following material parameters: nematic to isotropic clearing temperature 90.6°C, extraordinary refractive index n_e = 1.5817, ordinary refractive index n_o = 1.4822, $\Delta n = n_e - n_o = 0.0995$, dielectric anisotropy $\Delta\varepsilon = \varepsilon_{//}$ - $\varepsilon_{\perp}$ = -3.7, vertical dielectric constant $\varepsilon_{\perp}$ = 7.2, parallel dielectric constant $\varepsilon_{//}$ = 3.5, $k_{11} = 16.1 \times 10^{-7}$ dyn; $k_{22} = 8.0 \times 10^{-7}$ dyn; $k_{33} = 17.5 \times 10^{-7}$ dyn, rotational viscosity = 158cp, k_{11}, k_{22}, and k_{33} are the splay, twist and bend elastic constants. The LC alignment is vertical without pretilt angle for the IFF MVA mode, and a small 2-degree pretilt angle for the VA mode. For the VA mode, the LC rubbing direction is set at the 45/135 degree in azimuthal direction under anti-parallel geometry. Cell gap is 3.5 μm for IFF MVA and 3.0 μm for VA mode. The front and rear polarizers are along the 0-degree and 90-degree axes and form a standard crossed polarizer geometry. We assumed the light leakage under the crossed polarizer geometry is 0.01% and the transmission under parallel polarizer geometry is 50%. The thickness of the LC alignment layer (polyimide, PI) is assumed to be 100 nm with a 3.9 dielectric constant.

We considered a color LCD with red, green and blue stripe color filter arrangement. To prevent complication by the actual color filter spectrum, we used 625 nm, 550 nm and 450 nm respectively for the wavelength of red, green and blue color filter transmitted spectrum with 100% transmission ratio.

We calculated the optical transmission, contrast ratio, dynamics response and optical image and contour plots. To check the fringe field effects, we considered dot and frame inversion driving schemes, where the fringe field effects are larger in the dot inversion driving scheme. We show the optical images under the crossed polarizer to show the major difference between the dot- and frame-inversion driving schemes, and also between microdisplay and large direct-view geometries. We also considered the optical cross-talk effects by calculating the active matrix color stimuli (AMCS) value. The ACMS is defined as follows:

$$\text{AMCS} = 1 - (\text{TR} + \text{TB} + \text{TG} - 3\text{xTK})/(\text{TW} - \text{TK}) \quad (1)$$

$$\text{TW} = \text{Tran}(\text{RED V} = \text{on, GREEN V} = \text{on, BLUE V} = \text{on}) \quad (2)$$

$$\text{TK} = \text{Tran (RED V} = \text{off, GREEN V} = \text{off, BLUE V} = \text{off}) \quad (3)$$

$$\text{TR} = \text{Tran (RED V} = \text{on, GREEN V} = \text{off, BLUE V} = \text{off}) \quad (4)$$

$$\text{TG} = \text{Tran (RED V} = \text{off, GREEN V} = \text{on, BLUE V} = \text{off}) \quad (5)$$

$$\text{TB} = \text{Tran (RED V} = \text{off, GREEN V} = \text{off, BLUE V} = \text{on}). \quad (6)$$

In this paper, the Off voltage is 1 volt and On voltage is 5 volts. The ACMS parameters are larger in VA mode in the microdisplay geometry, indicating the larger cross-talk effects in VA in microdisplay geometry.

III. 3D LCD Modeling I: Microdislay VA AND IFF MVA LCDs With 3.75×11.25 μm Dot Size

3.1 Pixel Geometry

In the first application, we performed a 3D LCD modeling for the VA and IFF MVA LCDs for microdisplay geometry of a dot size of 3.75×11.25 μm, with a 60% aperture ratio. This is correspondent to a very high pixel density of 2258 pixels-per-inch (PPI). The pixel

opening area is 2.85×8.50 μm. The pixel density is very high and the intrinsic fringe field is very strong, this is good feature for the IFF MVA since it use the intrinsic fringe field to create the IFF MVA operation, but it make significant impact on the VA and create large disclination on the VA LC structures. The optical performance is summarized in table 1.

The fringe field effects induced large disclination in the VA microdisplay geometry, thus reducing their optical transmission. In the frame inversion driving scheme, the fringe field induced disclination is greatly reduced, thus the transmission for the frame inversion driving scheme is significantly larger than the VA under dot inversion driving scheme. However, the cross-talk effects (AMCS) are significantly larger in the frame inversion driving scheme in microdisplay geometry, as indicated by the large AMCS value. The switching-on response times in the VA under the frame inversion driving scheme are significantly longer by the larger cross-talk effects. For the IFF MVA, the optical transmission is greatly reduced by the central vertically aligned LC structure in the multi-domain LC structure. However, the circular polarizer improves the light transmission to be similar to that for the VA mode under dot inversion driving scheme. The cross-talk effects are small in the IFF MVA.

3.2 MVA Mode Operation under Dot Inversion Driving Scheme

The calculated results showed the IFF MVA transmission can be significantly enlarged (nearly doubled) by the circular polarizer. We calculate the results with and without the optical compensation and the results show that with the optical compensation film, the light leakage in the optical black state can be significantly reduced and the viewing angle cone is significantly enlarged as show on the CR contour plot.

Figure 1 shows the display performance under a crossed linear polarizer for (a) Field-on stats optical image; (b) Viewing angle contour plot for the field-off state transmittance; (c) Viewing angle contour plot for the field-on state transmittance; and (d) Viewing angle contour plot for the CR. A fan type characteristics image is shown for IFF MVA under the linear polarizer. The image is same as the regular fan type image that had been observed in the microdisplay geometry [5].

Figure 2 shows the IFF MVA display performance under a crossed circular polarizer for (a) Field-on stats optical image; (b) Viewing angle contour plot for the field-off state transmittance; (c) Viewing angle contour plot for the field-on state transmittance; and (d) Viewing angle contour plot for the CR. A circular dot type characteristics image is shown for IFF MVA under the circular polarizer. The transmission is improved from 1.38% for the linear polarizer to 3.03% for the circular polarizer. This is a 2.2-fold improvement.

Figure 3 shows the IFF MVA display performance under the crossed linear polarizer with an optical compensation film (negative birefringence with a vertically orientated optical axis, $\Delta n \times d = -$ 174nm, to match the LC $\Delta n \times d$) for (a) Viewing angle contour plot for the field-off state transmittance; (b) Viewing angle contour plot for the field-on state transmittance; and (c) Viewing angle contour plot for the CR. The field-on state optical image is similar to the uncompensated optical images [Fig 1(a)]. The results show that with the optical compensation film, light leakage in the optical black state can be significantly reduced and the CR contour plot can be significantly enlarged.

Figure 4 shows the IFF MVA display performance under a crossed circular polarizer with an optical compensation film (negative birefringence with a vertically orientated optical axis, $\Delta n \times d =$ - 174nm to match the LC $\Delta n \times d$) for (a) Viewing angle contour plot for the field-off state transmittance; (b) Viewing angle contour plot for the field-on state transmittance; and (c) Viewing angle contour plot for the CR. The field-on state optical image is similar to the uncompensated optical images [Fig 2(a)]. The results show that with

Table 1. Summary of the optical performance for the IFF MVA and VA modes, for the 3.75×11.25 μm dot. L-R denotes Left-to-Right and U-D denotes Up-to-Down

Microdisplay IFF MVA and VA Performance Summary: 3.75×11.25 μm Dot						
No	IFF MVA		VA (Dot)		VA (Frame)	
Driving Scheme	Dot		Dot		Frame	
Polarizer	Linear	Circular	Linear	Circular	Linear	Circular
Tran	1.38%	3.03%	1.98%	3.52%	2.64%	5.29%
CR	500	1100	720	1260	950	1880
Viewing Angle	Symmetrical		Asymmetrical			
Viewing Angle Cone (CR = 10)						
a. W/O Film	L-R: 85°-85° U-D: 85°-85°	L-R: 85°-85° U-D: 85°-85°	L-R: 85°-85° U-D: 85°-85°	L-R: 30°-25° U-D: 26°-28°	L-R: 85°-85° U-D: 85°-85°	L-R: 28°-28° U-D: 27°-33°
b. With Film (C-plate)	L-R: 85°-85° U-D: 85°-85°	L-R: 85°-85° U-D: 85°-85°	L-R: 85°-85° U-D: 85°-85°	L-R: 85°-85° U-D: 85°-85°	L-R: 85°-85° U-D: 85°-85°	L-R: 85°-85° U-D: 85°-85°
On time (0–90%, ms)	11.7	18.2	9.7	9.4	77.6	82.2
Off time (100–10%, ms)	1.9	3.2	3.0	3.0	5.1	4.6
AMCS	−0.45%	1.06%	−3.28%	−3.59%	8.33%	16.96%

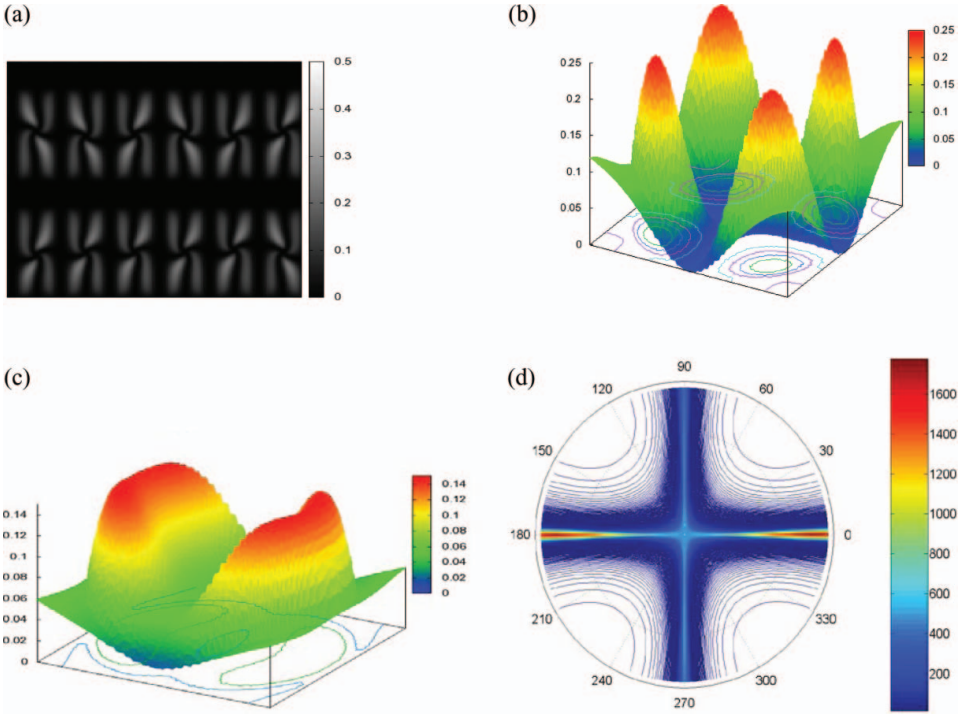

Figure 1. IFF MVA display performance under the dot inversion driving scheme and crossed linear polarizer for a dot size of 3.75 × 11.25 μm. (a) Field-on state optical image. (b) Viewing angle contour plot for the field-off state transmittance. (c) Viewing angle contour plot for the field-on state transmittance. (d) Viewing angle contour plot for the CR with full 180 degree viewing angle cone.

the optical compensation film, light leakage in the optical black state can be significantly reduced and the CR contour plot can be significantly enlarged. Also, because of the quarter wave plate, the axis for the best CR is also rotated by ∼10 degrees in the clockwise direction. Thus in the LCD application, the polarizer axis attachment angle on the LC panel needs to be changed from 0/90-degree to 10/100-degree so that the two best viewing angle axes are along the horizontal and vertical viewing angle zones.

The results show that stable IFF MVA operation can be obtained in the microdisplay geometry for the 3.75×11.25 μm dot size, the transmission can be enlarged by a circular polarizer, and the viewing angle can be enlarged by a negative birefringence compensation films.

3.3 VA Mode Operation under Dot Inversion and Frame Inversion Driving Schemes

The calculated results show a different VA structure and optical performance in both frame- and dot-inversion driving schemes as compared to their LC structure in the large direct-view pixel. These are the consequences from the strong fringe field in the small pixel geometry. We first discuss the VA mode operation under dot inversion driving scheme in section 3.3.1 and then follow the discussion for frame inversion driving scheme in Section 3.3.2.

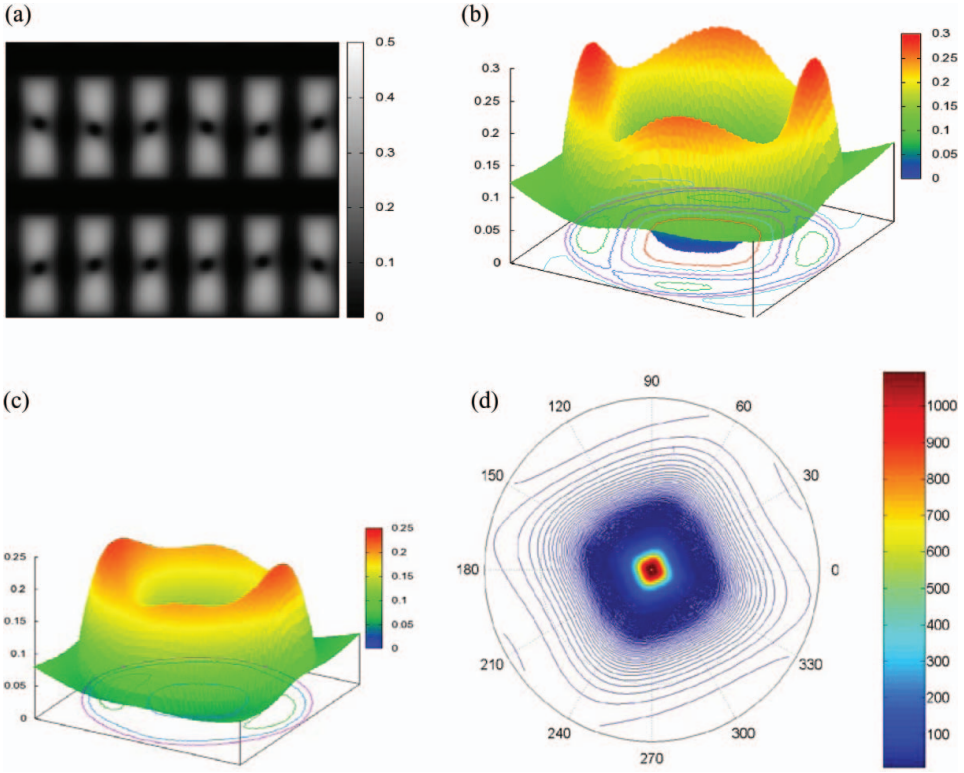

Figure 2. IFF MVA display performance under the dot inversion driving scheme and crossed circular polarizer for a dot size of 3.75 $\times$ 11.25 μm. (a) Field-on state optical image. (b) Viewing angle contour plot for the field-off state transmittance. (c) Viewing angle contour plot for the field-on state transmittance. (d) Viewing angle contour plot for the CR with full 180 degree viewing angle cone.

3.3.1 VA Mode Operation under Dot Inversion Driving Scheme. In this section, we discuss the VA operation under the dot inversion driving scheme. Figure 5 shows the VA display performance under the crossed linear polarizer for: (a) Field-on stats optical image; (b) Viewing angle (VA) contour plot for the field-off state transmittance; (c) Viewing angle contour plot for the field-on state transmittance; and (d) Viewing angle contour plot for the CR. A fan-type pattern is shown for VA under the linear polarizer where in Section 4.3.1, we showed that the regular VA mode in the large pixel size does not show the fan-type pattern. Figures 5(b) and 5(c) show asymmetrical viewing angle characteristics for the off and on states for the VA mode.

Figure 6 shows the VA display performance under a crossed circular polarizer for: (a) Field-on stats optical image; (b) Viewing angle contour plot for the field-off state transmittance; (c) Viewing angle contour plot for the field-on state transmittance; and (d) Viewing angle contour plot for the CR. A circular dot type image is shown for VA under the circular polarizer. This is a result of the significant impact from the VA structure under the strong fringe field, and it creates significant twist type orientation and also edge disclination in the small pixel geometry. In Section 4.3.2, we show that in the large pixel size, regular VA mode does not show the circular dot type image under circular polarizer. Figure 6(c) shows asymmetrical viewing angle characteristics for the field-on state. The transmission

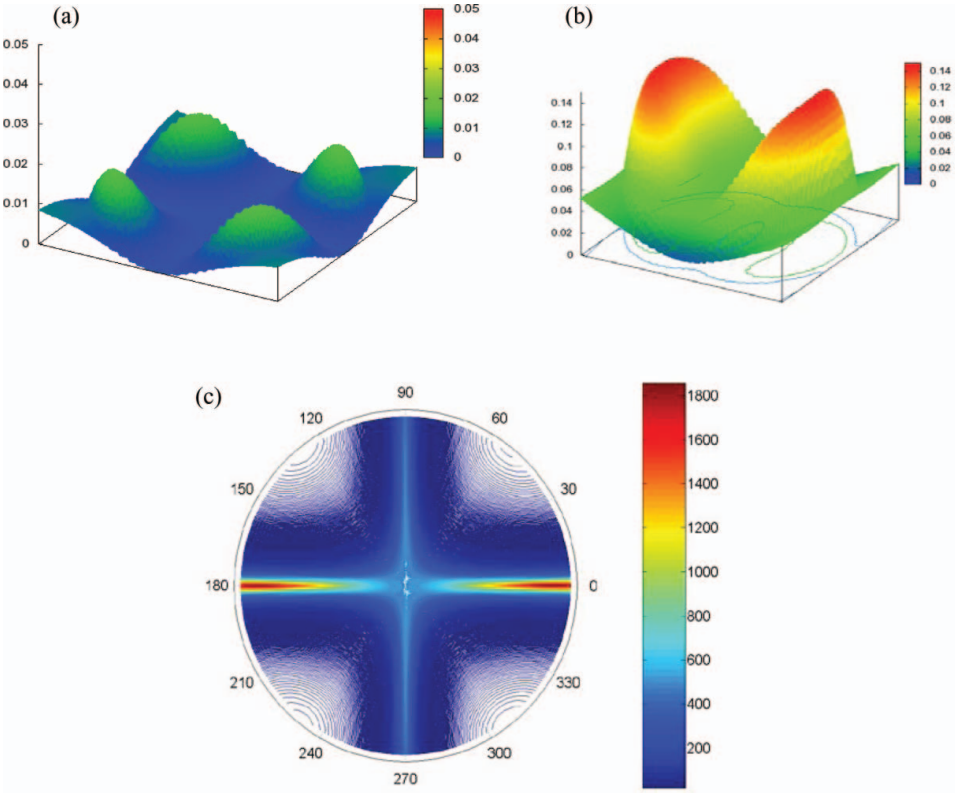

Figure 3. IFF MVA display performance under the dot inversion driving scheme and crossed linear polarizer with an optical compensation film for a dot size of 3.75 × 11.25 μm. (a) Viewing angle contour plot for the field-off state transmittance. (b) Viewing angle contour plot for the field-on state transmittance. (c) Viewing angle contour plot for the CR with full 180 degree viewing angle cone.

is improved from 1.98% for the linear polarizer to 3.52% for the circular polarizer. This is a 78% improvement.

3.3.2 VA Mode Operation under Frame Inversion Driving Scheme. In this section, we discuss the VA characteristics under the frame inversion driving scheme. Figure 7 shows the VA display performance under the crossed linear polarizer for: (a) Field-on stats optical image; (b) Viewing angle contour plot for the field-on state transmittance; and (c) Viewing angle contour plot for the CR. Contrary to the dot inversion driving scheme, a regular VA type characteristics image is shown, except with a large edge disclination. The viewing angle contour plot for the field-off state transmittance is the same as Fig. 5(b) for the dot inversion driving scheme. Figure 7(c) shows asymmetrical viewing angle characteristics for the on states for the VA mode.

Figure 8 shows the VA display performance under the crossed circular polarizer for: (a) Field-on stats optical image; (b) Viewing angle contour plot for the field-on state transmittance; and (c) Viewing angle contour plot for the CR. In contrast to the fan-type image in Fig. 6(a) for the dot inversion driving scheme, Fig. 8(a) shows a white image without circular dot type image. This is similar to the Fig. 16(a) for the white image for the large pixel size regular VA mode. The viewing angle contour plot for the field-off

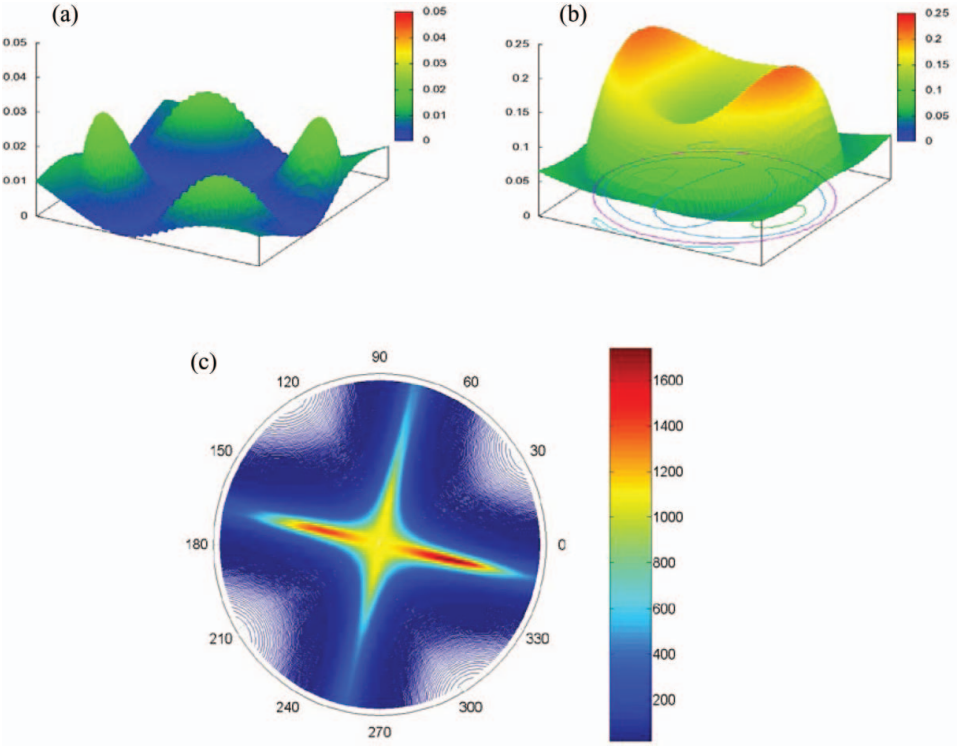

Figure 4. IFF MVA display performance under the dot inversion driving scheme and crossed circular polarizer with an optical compensation film for a dot size of 3.75 × 11.25 μm. (a) Viewing angle contour plot for the field-off state transmittance. (b) Viewing angle contour plot for the field-on state transmittance. (c) Viewing angle contour plot for the CR with full 180 degree viewing angle cone.

state transmittance is same as Fig. 6(b) for the dot inversion driving scheme. Figure 8(c) shows asymmetrical viewing angle characteristics for the field-on state. The transmission is improved from 2.64% for the linear polarizer to 5.29% for the circular polarizer. This is a big 101% improvement.

The results show VA mode in the microdisplay geometry is different from that for the direct-view pixel where the fringe fields impact the VA operation and optical performance. In the dot inversion driving scheme, VA mode shows a fan-type image. The transmission in both dot- and frame-inversion driving schemes can be improved by the circular polarizer, and the viewing angle can be enlarged by the negative birefringence compensation films. To reduce the fringe field effects, we use the frame inversion driving scheme, larger pretilt angle, and thinner cell gap. However all three methods can induce other optical effects which need to be properly considered.

IV. 3D LCD Modeling II: Direct-view Viewing Angle And Iff MVA LCDs WITH 63.2×189.6 μm Dot Size

4.1 Pixel Geometry

In the second application, we performed a 3D LCD modeling for the VA and IFF MVA LCDs for direct-view geometry of a dot size of 63.2×189.6 μm. This corresponds to a

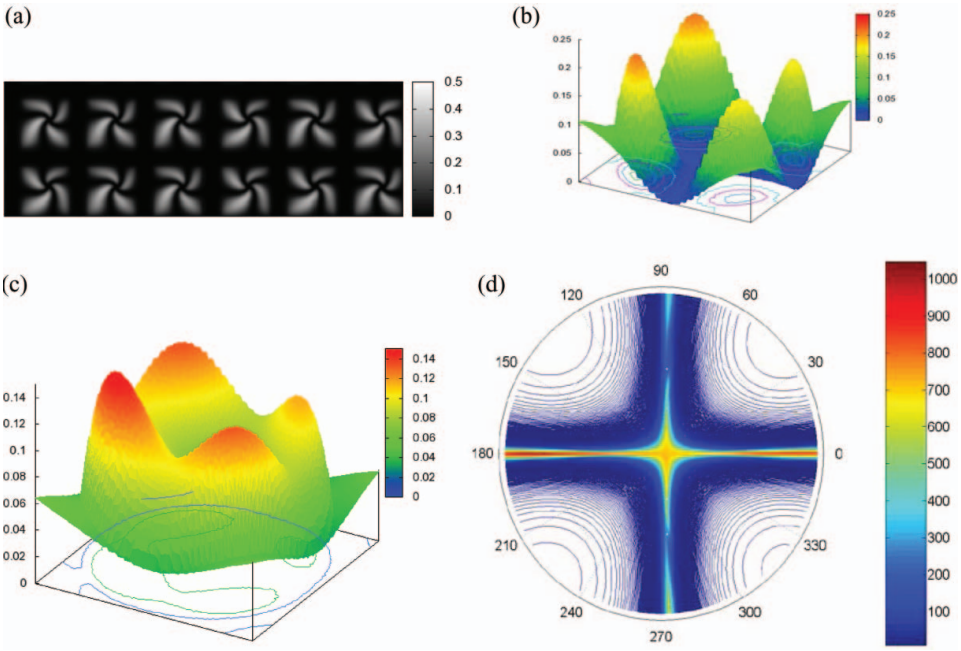

Figure 5. VA display performance under the dot inversion driving scheme and crossed linear polarizer for a dot size of 3.75 × 11.25 μm. (a) Field-on state optical image. (b) Viewing angle contour plot for the field-off state transmittance. (c) Viewing angle contour plot for the field-on state transmittance. (d) Viewing angle contour plot for the CR with full 180 degree viewing angle cone.

standard pixel density of 133 PPI for the small-medium size LCDs. The pixel opening area is 49.20×147.60 μm, with a 60% aperture ratio. The pixel is large and the intrinsic fringe field is weak, thus the IFF MVA is not stable in the direct-view geometry. We need the additional pixel designs to amplify the intrinsic fringe field to create a stable AIFF MVA operation [16–18]. Also, it makes a smaller impact on the VA and creates normal disclination on the edge in the VA LC structures. The fringe field effects are larger in the dot inversion driving scheme than the frame inversion driving scheme. The optical performances are summarized in Table 2.

The fringe field effects have induced disclination in the VA under dot inversion driving scheme and IFF MVA, thus reducing their optical transmission. It is interesting to know that the circular polarizer can have considerable improvement on the transmission for both the IFF MVA and VA, with 125% for IFF MVA, and 24% for VA under dot inversion driving scheme and 25% for VA under frame inversion driving scheme. In addition, the optimized transmission for the IFF MVA is the same as the transmission for the VA under dot- and frame-inversion driving schemes. This is a big difference in the results for the microdisplay geometry.

We calculated the results without the optical compensation film. As we showed in Section 3, we can use the optical compensation film to reduce the light leakage in the optical-black state and enlarge the viewing angle cone. For both normally-black IFF MVA and VA modes, the field-off states for the direct-view are the same as those for the microdisplay geometries. The reduction of the light leakage in the black state in large viewing angles by the optical compensation films can be applied for both direct-view and microdisplay.

Table 2. Summary of the optical performance for the IFF MVA and VA modes, for the 63.2×189.6 μm dot. L-R denotes Left-to-Right and U-D denotes Up-to-Down.

Direct-View IFF MVA and VA Performance Summary: 63.2×189.6 μm Dot						
No	IFF MVA		VA (Dot)		VA (Frame)	
Driving Scheme	Dot		Dot		Frame	
Polarizer	Linear	Circular	Linear	Circular	Linear	Circular
Tran	7.9%	26.5%	19.8%	24.5%	19.9%	24. 6%
CR	860	2890	2160	2630	2160	2630
Viewing Angle	Symmetrical		Asymmetrical			
Viewing Angle Cone (CR = 10)						
a. W/O Film	L-R: 85°-85° U-D: 85°-85°	L-R: 85°-85° U-D: 85°-85°	L-R: 85°-85° U-D: 85°-85°	L-R: 33°-29° U-D: 29°-31°	L-R: 85°-85° U-D: 85°-85°	L-R: 33°-29° U-D: 29°-31°
b. With Film (C-plate)	L-R: 85°-85° U-D: 85°-85°	L-R: 85°-85° U-D: 85°-85°	L-R: 85°-85° U-D: 85°-85°	L-R: 85°-85° U-D: 85°-85°	L-R: 85°-85° U-D: 85°-85°	L-R: 85°-85° U-D: 85°-85°
On time (0–90%, ms)	115.5	27.6	11.7	12.2	11.7	12.2
Off time (100–10%, ms)	12.2	3.2	3.0	3.0	5.1	4.6
AMCS	−1.77%	−0.08%	−0.04%	−0.04%	0.05%	0.04%

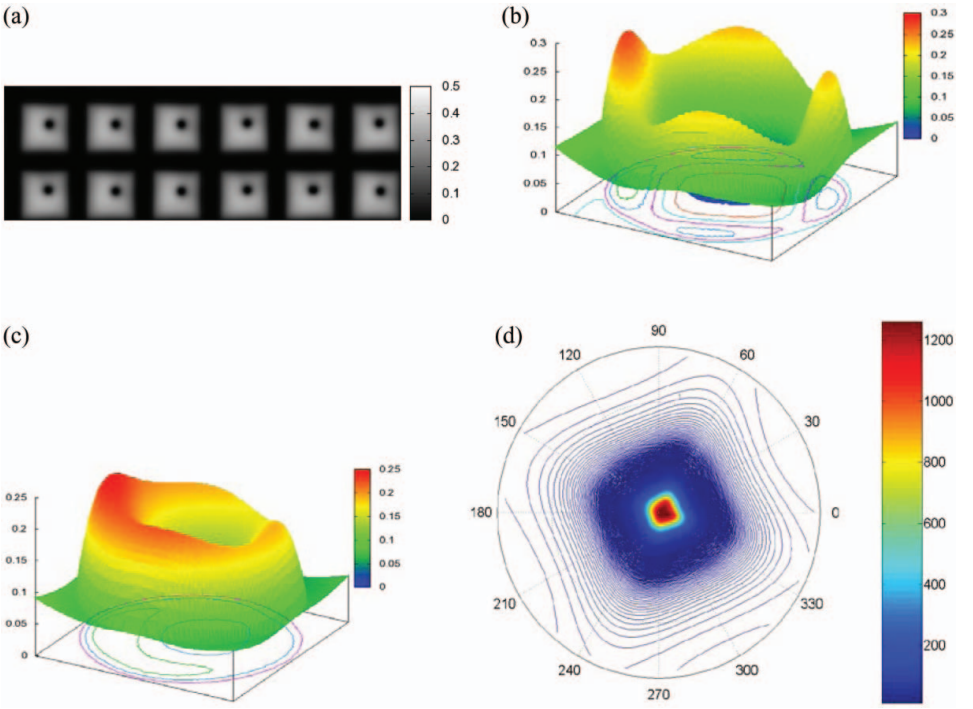

Figure 6. VA display performance under the dot inversion driving scheme and crossed circular polarizer for a dot size of 3.75 × 11.25 μm. (a) Field-on state optical image. (b) Viewing angle contour plot for the field-off state transmittance. (c) Viewing angle contour plot for the field-on state transmittance. (d) Viewing angle contour plot for the CR with full 180 degree viewing angle cone.

Thus the viewing angle can be significantly improved by the negative birefringence optical compensation films in both geometries, as we have discussed in Sections 3.2 and 3.3 for the microdisplay geometry. The viewing angle contour plots for the field-off state transmittance in the direct-view geometry is same as those for the microdisplay geometries, thus they will not be shown here.

The cross-talk effects are small, as indicated by the small AMCS values. The switching on response times in the IFF MVA are significantly longer. The IFF MVA is not stable in the large pixel geometry, but it can be made stable using the AIFF MVA designs [16–18].

4.2 IFF MVA Mode Operation under Dot Inversion Driving Scheme

The calculated results showed the IFF MVA transmission can be about doubled by the circular polarizer.

Figure 9 shows the display performance under the crossed linear polarizer for (a) Field-on stats optical image; (b) Viewing angle contour plot for the field-on state transmittance; and (c) Viewing angle contour plot for the CR. An image of irregular multi-disclination loops is shown for IFF MVA under the linear polarizer. Similar image is shown for the 45/135-degree linear polarizer geometry. The image is different from the regular fan type

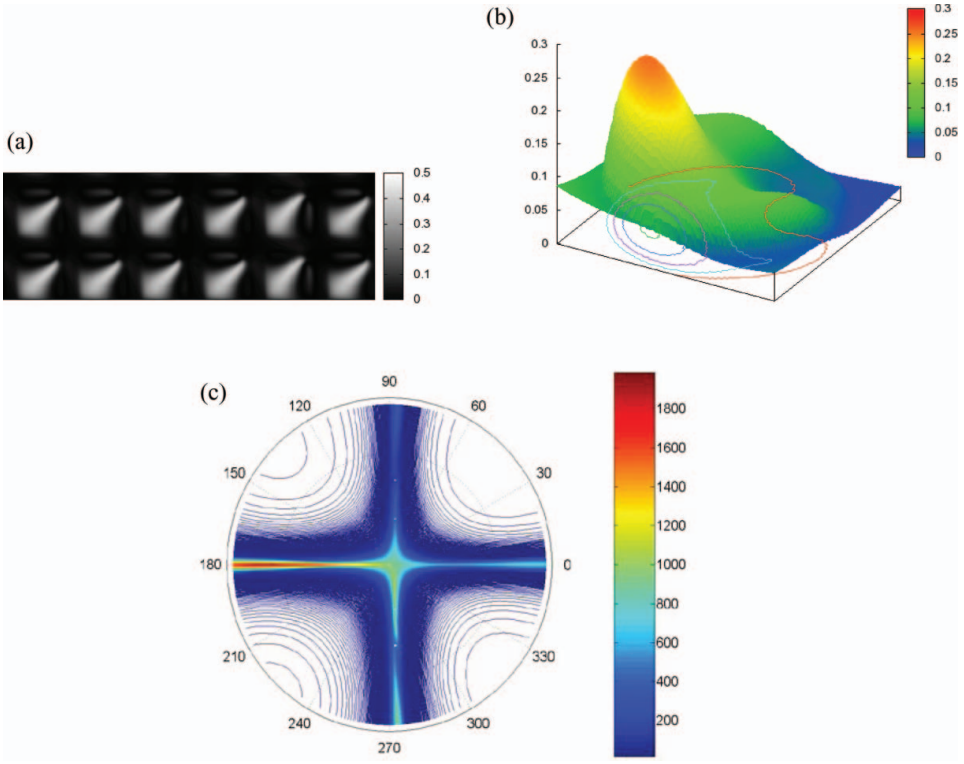

Figure 7. VA display performance under the frame inversion driving scheme and crossed linear polarizer for a dot size of 3.75 × 11.25 μm. (a) Field-on state optical image. (b) Viewing angle contour plot for the field-on state transmittance. (c) Viewing angle contour plot for the CR with full 180 degree viewing angle cone.

image that is observed in the microdisplay geometry and for the AIFF MVA in the direct-view geometry [5, 17]. This is caused by the unstable IFF MVA operation in the direct-view LCD.

Figure 10 shows the IFF MVA display performance under a crossed circular polarizer for (a) Field-on stats optical image; (b) Viewing angle contour plot for the field-off state transmittance; (c) Viewing angle contour plot for the field-on state transmittance; and (d) Viewing angle contour plot for the CR. Multiple circular-dot images are shown for IFF MVA under the circular polarizer. This image is different from the one-circular-dot type image for the IFF MVA under the microdisplay geometry and for the AIFF MVA in the direct-view geometry [5, 16–18]. This is caused by unstable IFF MVA operation in the direct-view LCD. The transmission is improved from 7.9% for the linear polarizer to 26.5% for the circular polarizer. This is a huge improvement.

Since the intrinsic fringe field is weak in the direct-view geometry, the IFF MVA is unstable, as evident from the following three results: an image of irregular multi- disclination loops under the crossed linear polarizer, the multiple-dots image under the crossed circular polarizer, and the very long switching-on response time in both linear (115.5ms) and circular polarizer (27.6ms). We need additional pixel designs to amplify the intrinsic fringe field to create a stable AIFF MVA operation [16–18].

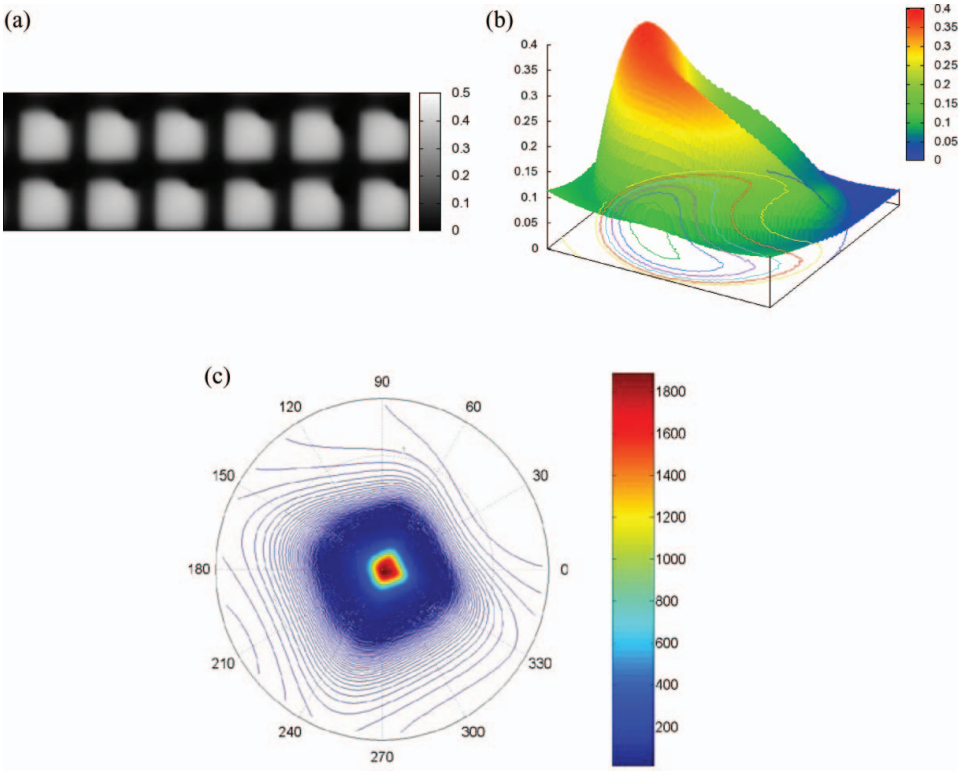

Figure 8. VA display performance under the frame inversion driving scheme and crossed circular polarizer for a dot size of 3.75 × 11.25 μm. (a) Field-on state optical image. (b) Viewing angle contour plot for the field-on state transmittance. (c) Viewing angle contour plot for the CR with full 180 degree viewing angle cone.

4.3 VA Mode Operation under Dot Inversion and Frame Inversion Driving Schemes

The calculated results showed that fringe field in this large direct-view pixel geometry has a small impact on the VA operation and it shows a different VA structure and optical performance in both frame- and dot-inversion driving schemes as compared to the VA mode in the small microdisplay pixel. We first discuss the VA mode operation under dot inversion driving scheme in section 4.3.1 and then follow with the discussion for frame inversion driving scheme in Section 4.3.2.

4.3.1 VA Mode Operation under Dot Inversion Driving Scheme. In this section, we discuss the VA operation under the dot inversion driving scheme. Figure 11 shows the VA display performance under a crossed linear polarizer for: (a) Field-on stats optical image; (b) Viewing angle contour plot for the field-off state transmittance; (c) Viewing angle contour plot for the field-on state transmittance; and (d) Viewing angle contour plot for the CR. A regular white characteristics image with a small edge disclination is shown in Fig 11(a) for VA under the linear polarizer. Figures 11(b) and (c) show asymmetrical viewing angle characteristics for the off and on states for the VA mode.

Figure 12 shows the VA display performance under the crossed circular polarizer for: (a) Field-on stats optical image; (b) Viewing angle contour plot for the field-off state transmittance; (c) Viewing angle contour plot for the field-on state transmittance; and (d) Viewing

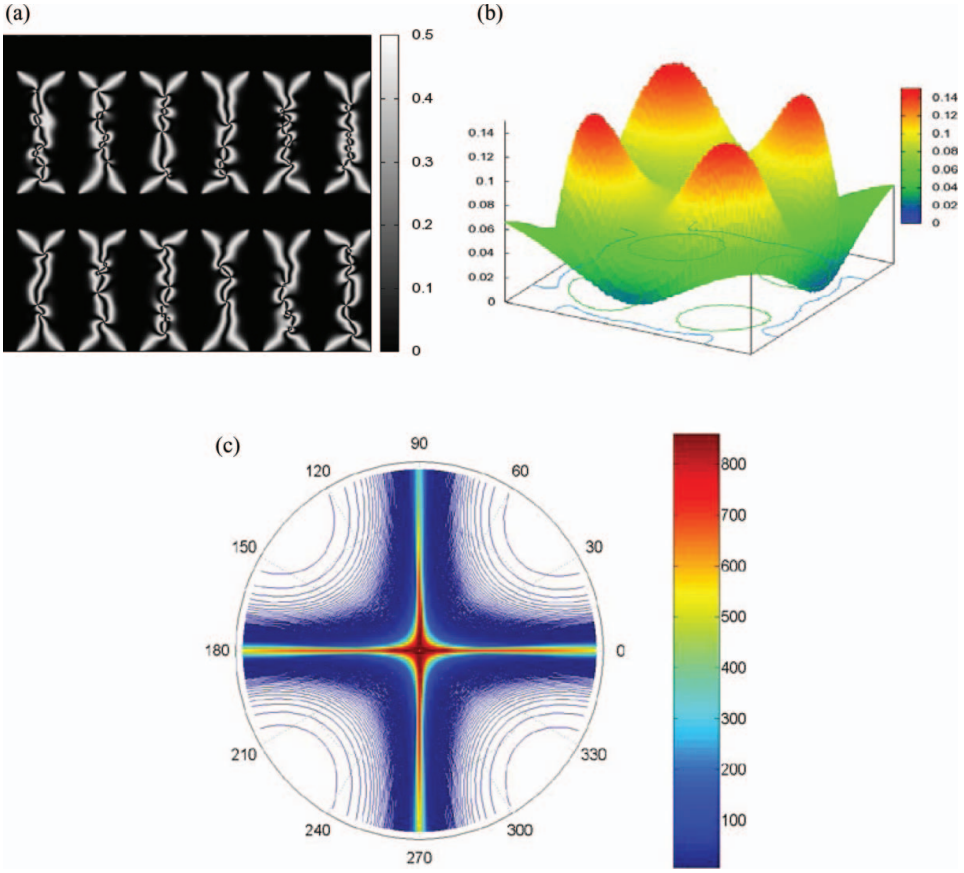

Figure 9. IFF MVA display performance under the dot inversion driving scheme and crossed linear polarizer for a dot size of 63.2 × 189.6 μm. (a) Field-on state optical image. (b) Viewing angle contour plot for the field-on state transmittance. (c) Viewing angle contour plot for the CR with full 180 degree viewing angle cone.

angle contour plot for the CR. A normal white characteristic image is shown in Fig 14(a). The VA mode under the circular polarizer also shows asymmetrical viewing angle characteristics for the on and off states. The transmission is improved from 19.83% for the linear polarizer to 24.54% for the circular polarizer. This is a 24% improvement.

4.3.2 VA Mode Operation under Frame Inversion Driving Scheme. In this section, we discuss the VA operation under the frame inversion driving scheme. Figure 13 shows the VA display performance under the crossed linear polarizer for: (a) Field-on stats optical image; (b) Viewing angle contour plot for the field-on state transmittance; and (c) Viewing angle contour plot for the CR. A regular VA type characteristics white image with one edge disclination is shown in Fig. 15(a). The viewing angle contour plot for the field-off state transmittance is the same as Fig. 5(b) for the dot inversion driving scheme. Figures 15(b) and (c) show asymmetrical viewing angle characteristics for the VA mode.

Figure 14 shows the VA display performance under the crossed circular polarizer for: (a) Field-on stats optical image; (b) Viewing angle contour plot for the field-on state transmittance; and (c) Viewing angle contour plot for the CR. A normal white characteristic

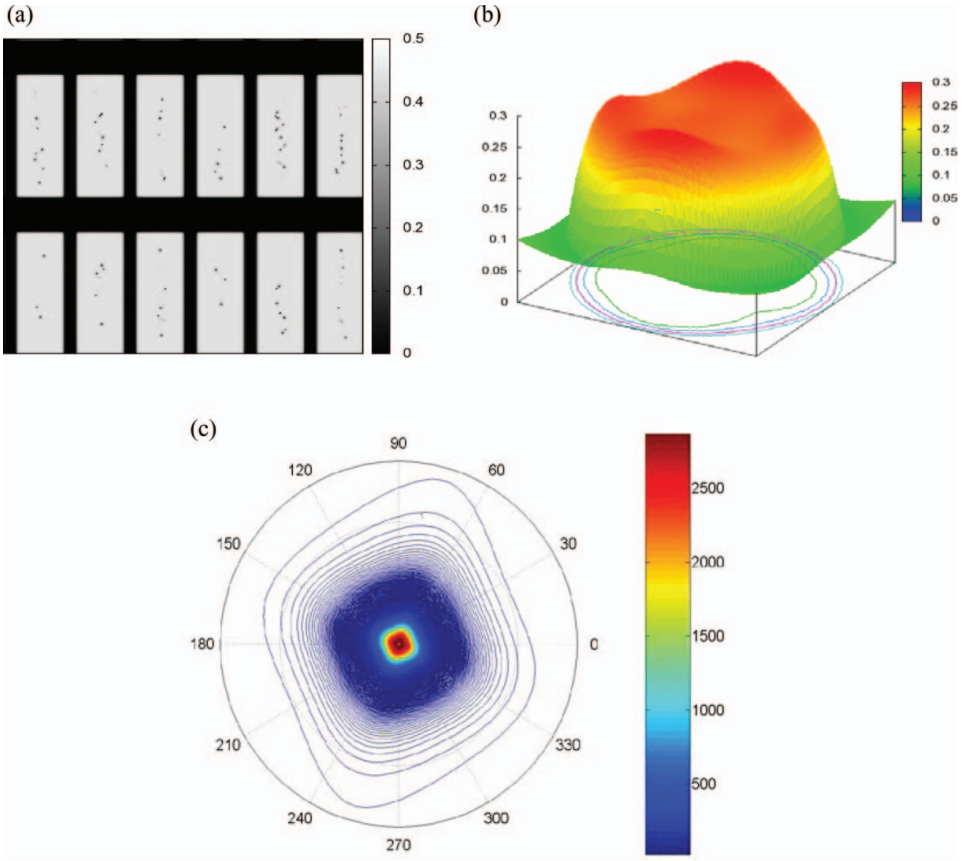

Figure 10. IFF MVA display performance under the dot inversion driving scheme and crossed circular polarizer for a dot size of 63.2 × 189.6 μm. (a) Field-on state optical image. (b) Viewing angle contour plot for the field-off state transmittance. (c) Viewing angle contour plot for the field-on state transmittance. (d) Viewing angle contour plot for the CR with full 180 degree viewing angle cone.

image is shown in Fig 16(a). The viewing angle contour plot for the field-off state transmittance is the same as Fig. 6(b) for the dot inversion driving scheme. The VA mode under the circular polarizer shows asymmetrical viewing angle characteristics for the on states. The transmission is improved from 19.85% for the linear polarizer to 24.56% for the circular polarizer. This is a 24% improvement.

The results show VA mode in the microdisplay geometry is different from the VA mode for the direct-view pixel where the strong fringe fields have impact the VA operation in microdisplay geometry. The transmission in both dot- and frame-inversion driving schemes can be significantly improved by the circular polarizer, and the viewing angle can also be enlarged by the negative birefringence compensation films.

V. Comparision Between Microdisplay and Direct-view Geometry

Except for the field-off states, there are major differences between the microdisplay and direct-view geometries. The transmission is significantly larger in the direct-view geometry

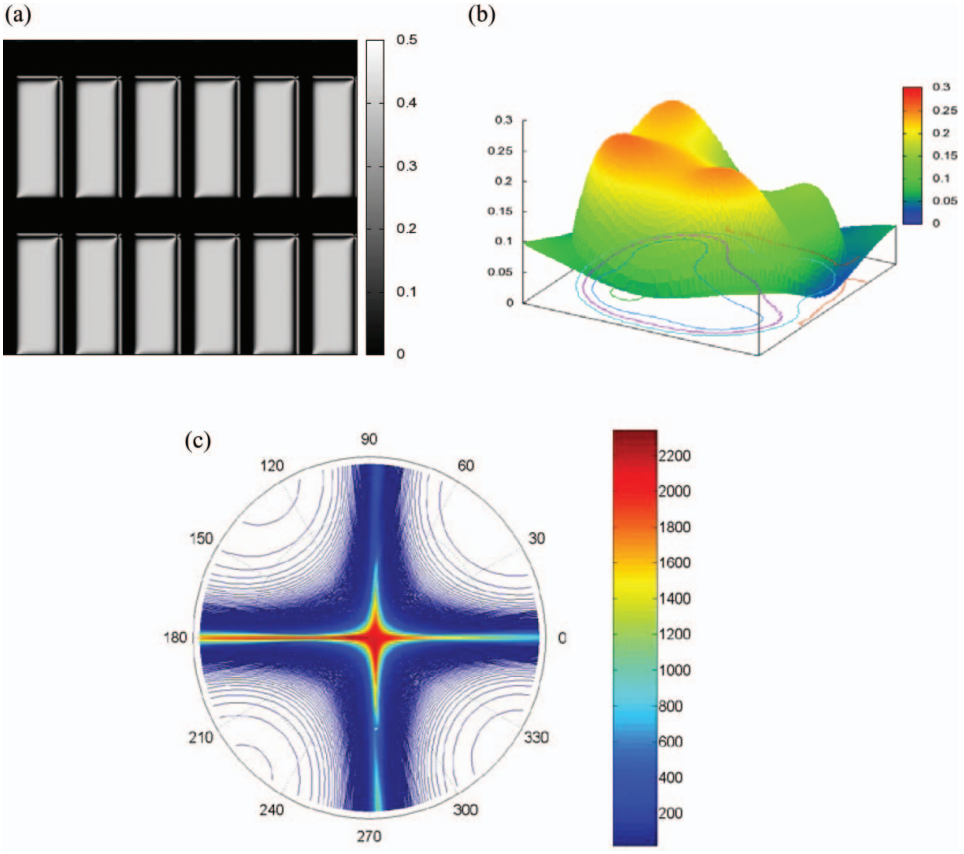

Figure 11. VA display performance under the dot inversion driving scheme and crossed linear polarizer for a dot size of 63.2 × 189.6 μm. (a) Field-on state optical image. (b) Viewing angle contour plot for the field-off state transmittance. (c) Viewing angle contour plot for the field-on state transmittance. (d) Viewing angle contour plot for the CR with full 180 degree viewing angle cone.

due to the smaller fringe field induced disclination effects, for both dot- and frame-inversion driving schemes. In particular, the transmissions under the circular polarizer are improved from 3.03%, 3.52% and 5.29% to 26.48%, 24.54% and 24.56% for the IFF MVA, VA with dot inversion driving scheme, and VA with frame inversion driving scheme respectively. The relative transmission improvements are 773%, 597%, and 364% respectively. This shows the large transmission reduction in the small display geometries from the fringe field.

Tables 1 and 2 show that the transmission for IFF MVA in microdisplay with the three to one aspect ratio pixel geometry is considerably lower than that for the VA mode under the frame inversion driving scheme (3.03% versus 5.29%); but the transmission for AIFF MVA in direct-view LCD could be make to similar to that for the VA mode under both the dot- and frame-inversion driving scheme (26.48% versus 24.56%). In addition, the transmission for IFF MVA in microdisplay could be further improved with a different pixel design and different aspect ratio. For example, we might further divide the 3.75×11.25 μm dot into 2 sub-dots. With 60% aperture ratio, the opening area is 2.90×4.36-um. Our studies show that the transmissions for the IFF MVA in the 2 sub-dots geometry are 3.2% and 5.8% for linear and circular polarizer respectively. Thus the transmission for IFF MVA is improved

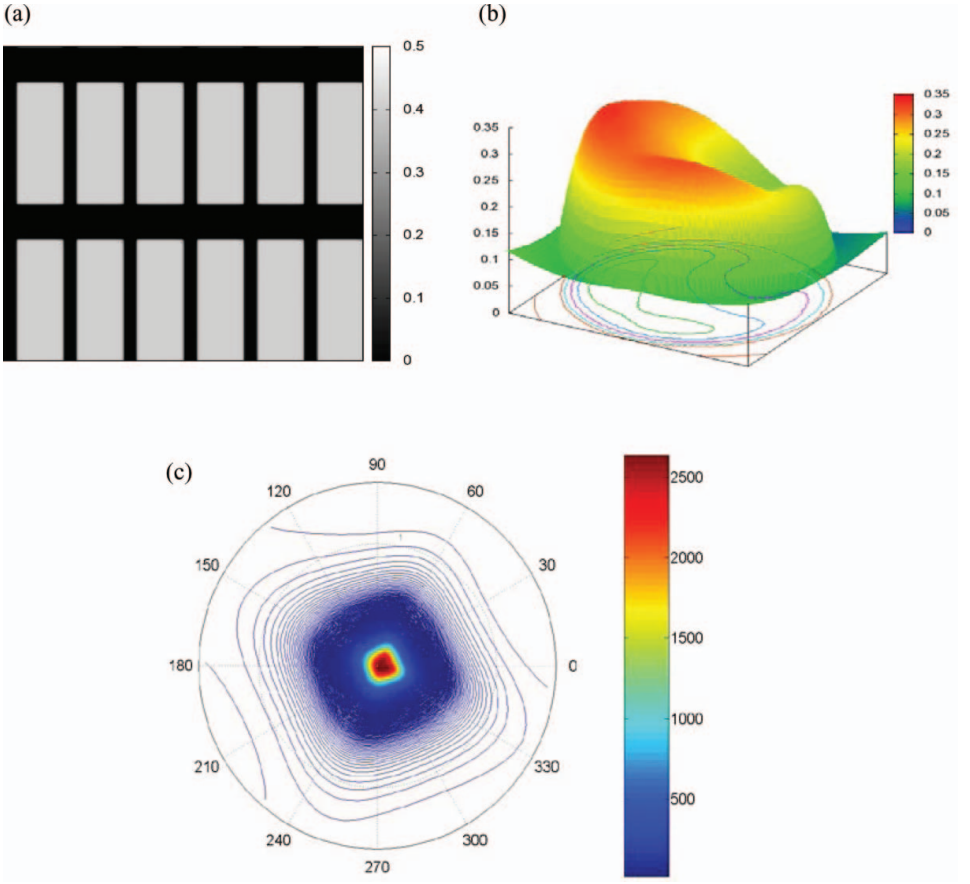

Figure 12. VA display performance under the dot inversion driving scheme and crossed circular polarizer for a dot size of 63.2 × 189.6 μm. (a) Field-on state optical image. (b) Viewing angle contour plot for the field-off state transmittance. (c) Viewing angle contour plot for the field-on state transmittance. (d) Viewing angle contour plot for the CR with full 180 degree viewing angle cone.

by 95% in the 2 sub-dots geometry as compared to the one dot geometry (5.9% versus 3.03%). The IFF MVA transmission for the 2 sub-dots is 12% larger than the transmission for the one-dot VA mode under the frame inversion driving scheme (5.9% versus 5.29%). In another geometry with the same total dot area, the 3.75×11.25 μm dot with a three to one aspect ratio could be changed to 5.625×7.5 um with a four-to-three aspect ratio pixel geometry. With 60% aperture ratio, the opening area is 4.67×5.24 um. Our studies showed that the transmissions for the IFF MVA in the 5.625×7.5 um dot are 5.9% and 10.4% for linear and circular polarizer respectively. Thus the transmission is improved by 243% in the 5.625×7.5um dot as compared to the 3.75×11.25 um dot (10.4% versus 3.03%). The IFF MVA transmission for the 5.625×7.5 um dot is even 97% larger than the transmission for the one-dot VA mode under the frame inversion driving scheme (10.4% versus 5.29%). These results are very important for the IFF MVA for both EVF and pico-projector applications. For EVF, the transmission, CR and viewing angle are important; whereas for pico-projectors, the transmission is the key factor while it is also important to have high CR and symmetrical viewing angle for the optical designs.

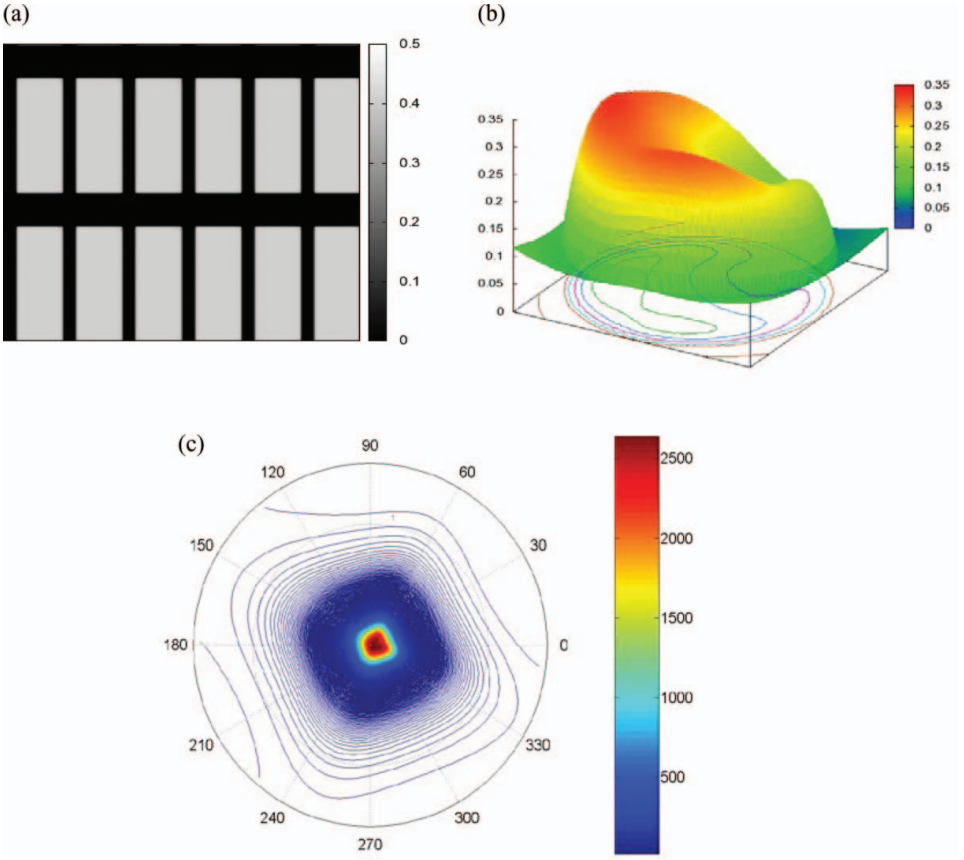

Figure 13. VA display performance under the frame inversion driving scheme and crossed linear polarizer for a dot size of 63.2 × 189.6 μm. (a) Field-on state optical image. (b) Viewing angle contour plot for the field-on state transmittance. (c) Viewing angle contour plot for the CR.

The response times are significantly different in both geometries. In particular, the response-on time for the IFF MVA are increased from 11.7-ms to 115.5-ms for the direct-view geometries, as a result of the unstable IFF MVA in the direct-view mode. In contrast, the response-on time for the VA under frame inversion driving scheme are reduced from 82.2-ms to 12.2-ms in the microdisplay to direct-view geometries, as a result of the more stable VA mode in the direct-view geometry.

The field-on state optical image is a good indicator of the LC structures. For the IFF MVA, under the linear and circular polarizers, the field-on state optical images [Figs 1(a) and 2(a)] in the microdisplay geometry show normal fan and one circular dot images, which are similar to the stable AIFF-MVA images. However, in the direct-view geometry, under the linear and circular polarizers, the IFF MVA shows irregular long disclination loops and many circular dot images, which are different to those stable AIFF MVA images. The response times and optical images show that the IFF MVA is stable in the microdisplay but un-stable in the direct-view geometry.

For the VA mode under the linear and circular polarizers, for both dot- and frame-inversion driving schemes, the field-on state optical images [Figs. 13(a), 14(a), 15(a) and 16(a)] in the direct-view geometry show regular small edge disclination images, without

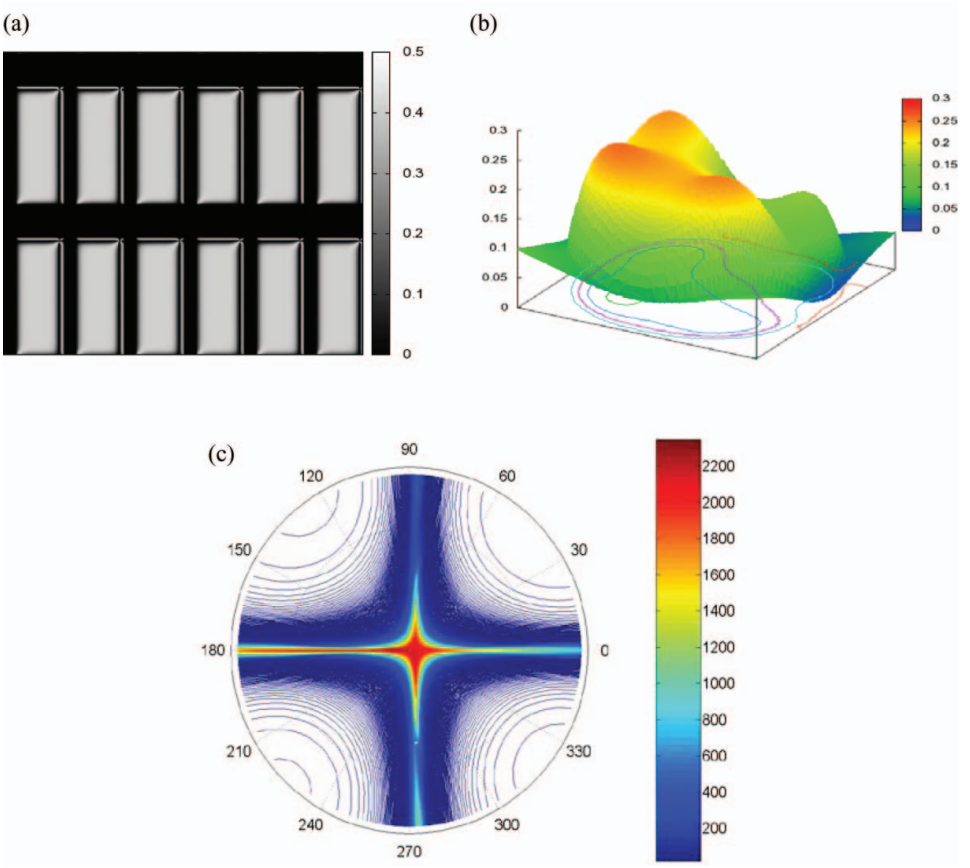

Figure 14. VA display performance under the frame inversion driving scheme and crossed circular polarizer for a dot size of 63.2 × 189.6 μm. (a) Field-on state optical image. (b) Viewing angle contour plot for the field-on state transmittance. (c) Viewing angle contour plot for the CR with full 180 degree viewing angle cone.

any fan-shaped or circular dots. However, in the microdisplay geometry, the VA with dot inversion driving scheme shows fan and one-circular dot images, similar to those in the IFF MVA; the VA with frame inversion driving scheme shows large edge disclination and LC twist structure images. The images are significantly different from those in the direct-view geometry, as a result of the large fringe field effects. With the long response time (82-ms) and large edge disclination optical image, the VA mode under frame inversion driving scheme is unstable in the microdisplay but stable in the direct-view geometry. Thus, proper stable IFF MVA operation is obtained in the microdisplay geometry, but it is unstable in the direct-view geometry, whereas regular VA operation is obtained in the direct-view geometry, but not in the microdisplay geometry.

VI. Conclusion

Our study showed a stable IFF MVA can be obtained in the microdisplay geometry but not in the large pixel size direct-view LCD geometry. This is consistent with experimental

fabrication results [5, 18, 19]. The results show insight into design of IFF MVA for the microdisplay and AIFF MVA for the large pixel size direct-view LCD applications. In particular, the transmission for IFF MVA with the three to one aspect ratio microdisplay is considerably lower than that for the VA mode under the frame inversion driving scheme; but the transmission for AIFF MVA in direct-view LCD could be made similar to that for the VA mode under both the dot- and frame-inversion driving scheme. In addition, the transmission for IFF MVA in microdisplay mode could be further improved with a different pixel design and different aspect ratio. In our first approach using a different pixel design of 2 sub-dots geometry, we showed that the transmission for the 2 sub-dots IFF MVA geometry is 12% larger than the transmission for the one-dot VA mode under the frame inversion driving scheme. In our second approach using a different four to three aspect ratio, the IFF MVA transmission for the 5.625×7.5 um dot with four to three aspect ratio is 97% larger than the VA transmission for the 3.75×11.25 um dot under the frame inversion driving scheme. Our study also showed a regular VA operation can be obtained in the direct-view LCD, but not in the microdisplay geometry. The results showed a small crossed talk and small edge disclination images from the LC reverse titled orientation for the direct-view VA LCD, but a large crossed-talk, large LC reverse titled combined with large twist orientation for the microdisplay VA geometry [15, 20–24]. This is consistent with experimental observation results. The results showed that VA with the dot-inversion driving scheme should be used for the direct-view geometry, but cannot be used for the microdisplay geometry. VA with the frame-inversion driving scheme should be used for the microdisplay geometry, with a greater frame rate required to reduce the flicker. Our 3D LCD program can be combined with the 3D LCD visual system to have a complete modeling system for the 3D LCD visual system applications, enhancing the design and operation of the VA mode for direct-view LCD and microdisplay pico-projector applications.

In conclusion, we have successfully developed a useful 3D LCD modeling program using the Q-tensor model for the LC orientation and 2×2 program matrix for the LC optical properties. We applied the program to calculate electro-optical properties for the VA and IFF MVA in the microdisplay and direct-view LCD geometries.

Acknowledgements

The authors are grateful to the National Science Council of the Republic of China and Kyoritsu Optronics Co., Ltd. for the financial support on this program under contract No. NSC 98-2622-E-001-001-CC2 and NSC 99-2622-E-001-001-CC2. We thank Dr Ronald P. Gale for a critical review of and suggestions on this paper.

References

[1] Tech Wiz LCD 3D AMLCD Simulation Tool, by SANAYI System Co., Ltd., #705, Daelim Bldg., Dohwa 1-dong, Nam-gu INCHEON, KOREA. www.sanayisystem.com.

[2] Expert, LCD, Daouxilicon, 7F, Daou Digital Square, 23–7, Jukjeon-dong, Suji-gu, Yonginsi, Gyeonggi-do, Korea 448–547. www.daouxilicon.com

[3] DIMOS LCD modeling software. AUTRONIC-MELCHERS GmbH. Greschbachstr. 29. D-76229 Karlsruhe. Germany. www.autronic-melchers.com

[4] LCD MASTER, Sintech, Inc. 90 Ogo-oku, Tabuse-Cho, Kumage-Gun, Yamaguchi-Ken, 742–1512, Japan. www.shintech.jp

[5] Ong, H. L., Cheong, N., Lo, J., Metras, M., Woodard, O., and Gale, R. P., SID'2005, p. 646–649 (2005).

[6] Ong, H. L. and Gale, R., Information Displays, Vol. *14*, no. 12, p. 18 (1998).

[7] Ong, H. L., International Display Research Conference 2000 Record, p. 8–12 (2000).
[8] De Gennes, P. G. and Prost, J., *The Physics of Liquid Crystals, 2nd ed.*, Clarebdon, Oxford (1993).
[9] Mori, H., Gartland, E. C., Jr., Kelly, J. R. and Bos, P. J., *Jpn. J. Appl. Phys. 38*, 135 (1999).
[10] Anderson, J., Watson, P., and Bos, P., *Liquid Crystals 28*, 109–115 (2001).
[11] Ho, I. L., Lin, M. C., Chen, C. D., Li, W. Y. and Hsu, H. K. (in press).
[12] Rokushima, K. and Yamakita, J., *J. Opt. Soc. Am. 73*, 901 (1983). Glytsis, E. N. and Gaylord, T. K., *J. Opt. Soc. Am. A 4*, 2061 (1987).
[13] Lien, A., *Liquid Crystals*, Vol. *22*, No. 2, 171–175 (1997).
[14] Ong, H. L., *J. Opt. Soc. Am. A 10*(2), p. 283 (1993).
[15] Lueder, E., *Liquid Crystal Displays*, John Wiley & Sons, Ltd., Chichester (2001).
[16] Ong, H. L. and Chou, J., 2005 *EuroDisplay*, p. 564–567 (2005).
[17] Ong, H. L., Chou, J., Wang, X. Y., Qiao, Y. B., Chiu, Y. W., Chung, D. C., and Jen, T. S., IDW'2010, p. 1083–1086 (2010).
[18] Ong, H. L. and Chou, J., SID'11, p. 58–61 (2011).
[19] Iwamoto, Y., Toko, Y., Hiramoto, H. and Iimura, Y., SID'00, p. 902–905 (2000).
[20] Ji, Y., Gandhi, J. and Stefanov, M. E., SID'99, p. 750–753 (1999).
[21] Cheng, C., Bos, P. J., Kim, J., Li, Q., Anderson, J. E., *J. Appl. Phys. 99*, No. 12, 123523-1-6, (2006).
[22] Chen, C., Anderson, J. E., Bos, P. J., *Jpn. J. Appl. Phys., Part 2 (Letters). 44*, N0.33–36, L1126–7, (2005).
[23] Vithana, H., Johnson, D., Bos, P., Herke, R., Fung, Y., Jamal, S., *Jpn. J. Appl. Phys. 35*, 2222 (1996).
[24] Vithana, H., Johnson, D., Bos, P., *Jpn. J. Appl. Phys. 35*, L320, (1996).